AGU PUBLICATIONS

Global Biogeochemical Cycles

RESEARCH ARTICLE

Key Points:
- Carbon isotope contents of photosynthesis and respiration differ
- Isotope fractionation of land photosynthesis dominates over the ^{13}C Suess effect
- Biogeochemical C isotope models must include terrestrial ecological processes

Ecological processes dominate the ^{13}C land disequilibrium in a Rocky Mountain subalpine forest

D. R. Bowling[1], A. P. Ballantyne[2], J. B. Miller[3,4], S. P. Burns[5,6], T. J. Conway[3], O. Menzer[7], B. B. Stephens[6], and B. H. Vaughn[8]

[1]Department of Biology, University of Utah, Salt Lake City, Utah, USA, [2]Department of Ecosystem and Conservation Science, University of Montana, Missoula, Montana, USA, [3]Earth System Research Laboratory, NOAA, Boulder, Colorado, USA, [4]Cooperative Institute for Research in Environmental Sciences, University of Colorado Boulder, Boulder, Colorado, USA, [5]Department of Geography, University of Colorado Boulder, Boulder, Colorado, USA, [6]National Center for Atmospheric Research, Boulder, Colorado, USA, [7]Department of Geography, University of California, Santa Barbara, California, USA, [8]Institute for Arctic and Alpine Research, University of Colorado Boulder, Boulder, Colorado, USA

Abstract Fossil fuel combustion has increased atmospheric CO_2 by ≈ 115 μmol mol^{-1} since 1750 and decreased its carbon isotope composition (δ^{13}C) by 1.7–2‰ (the ^{13}C Suess effect). Because carbon is stored in the terrestrial biosphere for decades and longer, the δ^{13}C of CO_2 released by terrestrial ecosystems is expected to differ from the δ^{13}C of CO_2 assimilated by land plants during photosynthesis. This isotopic difference between land-atmosphere respiration (δ_R) and photosynthetic assimilation (δ_A) fluxes gives rise to the ^{13}C land disequilibrium (*D*). Contemporary understanding suggests that over annual and longer time scales, *D* is determined primarily by the Suess effect, and thus, *D* is generally positive ($\delta_R > \delta_A$). A 7 year record of biosphere-atmosphere carbon exchange was used to evaluate the seasonality of δ_A and δ_R, and the ^{13}C land disequilibrium, in a subalpine conifer forest. A novel isotopic mixing model was employed to determine the δ^{13}C of net land-atmosphere exchange during day and night and combined with tower-based flux observations to assess δ_A and δ_R. The disequilibrium varied seasonally and when flux-weighted was opposite in sign than expected from the Suess effect ($D = -0.75 \pm 0.21$‰ or -0.88 ± 0.10‰ depending on method). Seasonality in *D* appeared to be driven by photosynthetic discrimination (Δ_{canopy}) responding to environmental factors. Possible explanations for negative *D* include (1) changes in Δ_{canopy} over decades as CO_2 and temperature have risen, and/or (2) post-photosynthetic fractionation processes leading to sequestration of isotopically enriched carbon in long-lived pools like wood and soil.

1. Introduction

The continuing increase of atmospheric CO_2 is resulting in physical, chemical, and biological impacts on the Earth system [*Falkowski et al.*, 2000]. However, at present, about half of the potential atmospheric rise is being offset by increasing net carbon uptake in the terrestrial biosphere and the oceans [*Ballantyne et al.*, 2012]. On land, carbon uptake by gross primary productivity (GPP) [*Beer et al.*, 2010; *Welp et al.*, 2011] slightly exceeds carbon loss due to respiration (R_{eco}) resulting in a net sink of carbon in the land biosphere [*Pan et al.*, 2011]. However, the environmental factors that control GPP and R_{eco} are distinct and changing through time, and projections of future carbon sinks remain uncertain due to gaps in understanding of these processes [*Friedlingstein et al.*, 2006; *Le Quere et al.*, 2009; *Schuur et al.*, 2008]. Hence, process-based investigations are critical to elucidate the major controls on carbon exchange between the biosphere and the atmosphere.

Combustion of fossil fuels adds CO_2 to the atmosphere that contains no radiocarbon because the fuels (coal, oil, gas, etc.) are old enough for ^{14}C to have radioactively decayed [*Levin et al.*, 2008]. In the 1950s, Hans Suess realized that not only the addition of ^{14}C-free CO_2 to the air altered the atmospheric ^{14}C/^{12}C ratio but that this change was recorded in wood [*Suess*, 1955]. Shortly after, Suess and Roger Revelle discovered that the radiocarbon signal also diluted the ^{14}C composition of dissolved inorganic carbon in the oceans [*Revelle and Suess*, 1957]. The ^{14}C dilution process in the atmosphere and oceans has come to be known as the Suess effect.

The fossil fuel combustion flux is also depleted in its stable ^{13}C/^{12}C isotope composition (δ^{13}C) relative to CO_2 in the air [*Bush et al.*, 2007]. Firn and ice core records indicate that as CO_2 has increased, the δ^{13}C of atmospheric

CO_2 has decreased by 1.7–2‰ [*Francey et al.*, 1999]. *Keeling* [1979] extended the use of the term Suess effect to indicate any change in ^{13}C or ^{14}C in any carbon cycle reservoir due to anthropogenic activities, and we will use "Suess effect" here to refer to the $\delta^{13}C$ change.

The $\delta^{13}C$ of plants reflects the isotopic composition of atmospheric CO_2 but additionally modified by the process of photosynthesis [*Cernusak et al.*, 2013]. Assuming that photosynthetic carbon isotope discrimination (which we will call Δ_{canopy}) has not changed since 1750, the Suess effect should cause an imbalance in the isotopic content of the contemporary photosynthetic and respiratory fluxes of the land biosphere [*Tans et al.*, 1993; *Yakir*, 2004]. For example, the $\delta^{13}C$ of atmospheric CO_2 was about −6.4‰ in 1750 [*Francey et al.*, 1999] and in 2012 was −8.4‰ in the Northern Hemisphere (as we will show later). If the global mean Δ_{canopy} is 18‰ and has been constant, then the $\delta^{13}C$ of the products of photosynthesis in 1750 was on average −24.4‰ and in 2012 was −26.4‰. We know from bomb radiocarbon and stable isotope studies that the residence time of carbon in the terrestrial biosphere varies from minutes to decades to centuries [*Frank et al.*, 2012; *Neill et al.*, 1996; *Schimel et al.*, 1994; *Trumbore*, 2009]. Since a significant amount of the contemporary respiration flux is derived from older carbon that is relatively more enriched in ^{13}C, the Suess effect should lead to a difference in the isotopic composition of the current photosynthesis flux (δ_A) and the respiration flux (δ_R) [*Naegler and Levin*, 2009; *Yakir*, 2004]. This imbalance is termed the ^{13}C land disequilibrium (*D*). The net ocean-atmosphere exchange is also isotopically imbalanced; both land and ocean disequilibria are important in using ^{13}C to partition the net carbon sinks between land and oceans using the double deconvolution approach [*Alden et al.*, 2010; *Ciais et al.*, 1995; *Joos and Bruno*, 1998; *Randerson et al.*, 2002; *Still et al.*, 2003].

Biogeochemical models that incorporate the Suess effect and long-lived carbon pools in the terrestrial biosphere [*Scholze et al.*, 2003; *van der Velde et al.*, 2013] predict that δ_R should be more enriched in ^{13}C (less negative $\delta^{13}C$) than δ_A over periods of several years or more. The magnitude of the disequilibrium over space and time varies primarily as a function of the residence time of carbon in long-lived pools like wood and soil. This leads to spatial variation in modeled *D* in different ecosystems, which is most pronounced with latitude [*Ciais et al.*, 1999; *Fung et al.*, 1997]. Regardless of location, the Suess effect-induced disequilibria tend to be small ($< 1‰$) with δ_R more enriched than δ_A. While some models allow for changes in Δ_{canopy} at time scales from minutes to decades that can potentially help us understand seasonal and spatial patterns in *D* [*Scholze et al.*, 2003; *van der Velde et al.*, 2013], these models only address isotopic effects during photosynthesis, ignoring possible fractionation as carbon moves through ecosystem pools or back to the atmosphere via respiration.

There is now substantial evidence that post-photosynthetic ^{13}C fractionation processes are important in terrestrial ecosystem carbon cycling, with isotopic changes that are much larger than the modeled terrestrial disequilibria [*Bowling et al.*, 2008; *Brüggemann et al.*, 2011; *Werner and Gessler*, 2011]. While we know that the Suess effect must contribute to *D*, these review papers highlight other ecological processes that may contribute to *D* at various time scales. Hence, a detailed investigation into the processes impacting the ^{13}C land disequilibrium is needed. There are several hundred sites around the world where net land-atmosphere CO_2 exchange has been monitored (as net ecosystem exchange, NEE) using tower-based observations for many years [*Baldocchi et al.*, 2001; *Mahecha et al.*, 2010; *Schwalm et al.*, 2010; *Stoy et al.*, 2009]. However, only a small subset of these sites includes concurrent observations the $\delta^{13}C$ of atmospheric CO_2 [*Flanagan et al.*, 2012; *Hemming et al.*, 2005; *Lai et al.*, 2005].

Here we describe a 7 year study of land-atmosphere CO_2 exchange and its carbon isotopic composition in a subalpine forest and a nearby alpine tundra ecosystem. The analysis presented utilizes the longest standing continuous observations of $\delta^{13}C$ of CO_2 at a flux tower site [*Riveros-Iregui et al.*, 2011; *Schaeffer et al.*, 2008b]. Our goal was to directly monitor the ^{13}C land disequilibrium in this forest and evaluate how it responded to seasonal environmental forcing. We examine the working hypothesis that the Suess effect is the dominant factor influencing the isotopic composition of biosphere-atmosphere CO_2 exchange fluxes.

2. Methods

2.1. Site Description

This study was conducted in the mountains at Niwot Ridge, Colorado, about 50 km northwest of the Denver, Colorado metropolitan area. Measurements were made at two nearby locations over 7 years (2006 to 2012 inclusive). The forest site (40.03°N, 105.55°W, 3050 m above sea level (masl)) was the Niwot Ridge AmeriFlux

forest [*Hu et al.*, 2010a], a subalpine forest dominated by the conifer species *Pinus contorta*, *Picea engelmannii*, and *Abies lasiocarpa* [*Monson et al.*, 2010]. The forest was harvested in the early 1900s and has not experienced a major disturbance since. During our study, the mountain pine beetle (*Dendroctonus ponderosae*) was present [*Mitton and Ferrenberg*, 2012] but tree mortality was negligible, in contrast to nearby forests with high mortality [*Rhoades et al.*, 2013]. The tundra site (historically called T-van [*Greenland*, 1989]) was located higher on Niwot Ridge, ≈4 km northwest of the forest site, and above tree line in the alpine tundra (40.05°N, 105.58°W, 3423 masl). Further details about the sites are available elsewhere [*Knowles et al.*, 2012; *Monson et al.*, 2002].

2.2. Carbon Dioxide and Stable Isotopes
2.2.1. Tundra Site Flasks

Carbon dioxide and $\delta^{13}C$ of CO_2 were monitored at the tundra site using weekly midday collections in glass flasks as part of the National Oceanic and Atmospheric Administration (NOAA)/Earth System Research Laboratory (ESRL)/Global Monitoring Division Carbon Cycle Greenhouse Gases Cooperative Air Sampling Network (http://www.esrl.noaa.gov/gmd/ccgg/). This record began at Niwot Ridge (NOAA site code NWR) for CO_2 in 1968 and for $\delta^{13}C$ of CO_2 in 1990. CO_2 in the flasks was measured using nondispersive infrared (NDIR) gas analysis at the NOAA laboratory [*Conway et al.*, 1994], and $\delta^{13}C$ of CO_2 using isotope ratio mass spectrometry (IRMS) at the Stable Isotope Laboratory of the University of Colorado's Institute for Arctic and Alpine Research [*Vaughn et al.*, 2004]. Precision for CO_2 and $\delta^{13}C$ for the flasks was 0.1 μmol mol^{-1} and 0.01‰.

2.2.2. Tundra Site Continuous

In summer 2005, an NDIR analyzer (AIRCOA) was installed at the tundra site for continuous observation of CO_2 [*Stephens et al.*, 2011]. Niwot Ridge is one site in a network of AIRCOAs located across the western U.S. Rocky Mountains [*Brooks et al.*, 2012; *Desai et al.*, 2011]. Air was sampled from three heights on a short mast every 2.5 min; hourly averages at the 5.1 m height above ground are reported here. Precision of these measurements was 0.1 μmol mol^{-1}.

2.2.3. Forest Site Continuous

A tunable diode laser absorption spectrometer (TDL [*Schaeffer et al.*, 2008a]) has been used since fall 2005 to continuously monitor CO_2 and $\delta^{13}C$ of CO_2 in forest air with precision of 0.2 μmol mol^{-1} and 0.25‰, respectively. Both quantities were measured at nine forest heights every 10 min and hourly/half-hourly averages of these data were used here. During some years, only the first half of a given hourly period was devoted to air measurements as described, and the instrument was used for other experiments during the second half of the hour. These data were used on a monthly basis to determine isotopic mixing relationships described below. The vegetation canopy during this study was 11–12 m tall. Measurements were made at 0.1, 0.5, 1, 2, 5, 7, 9, and 11 m above the ground, and at the eddy covariance measurement height (21.5 m, described below). There was little understory vegetation.

In all cases, CO_2 is reported relative to the World Meteorological Organization Mole Fraction Scale (WMO X2007), and $\delta^{13}C$ of CO_2 relative to the International Atomic Energy Agency Vienna Pee Dee Belemnite (VPDB) Scale. Field-based measurements were linked to these scales using custom compressed gas standards via NDIR and IRMS at the Stable Isotope Ratio Facility for Environmental Research at the University of Utah and the National Center for Atmospheric Research.

2.3. Biosphere/Atmosphere Fluxes and Climate

Fluxes of CO_2 (net ecosystem exchange or NEE), H_2O, and energy have been monitored half-hourly at the Niwot Ridge AmeriFlux forest using eddy covariance at 21.5 m height since 1998 [*Hu et al.*, 2010a; *Monson et al.*, 2002]. Standard environmental and weather variables have been measured at the forest since 1998. Relevant measurements for this study include global radiation, air and soil temperature, vapor pressure deficit of air, and soil moisture.

Observations of NEE at the forest site provide the net CO_2 exchange between the forest and the atmosphere. The biological processes of gross primary production (GPP, also called gross photosynthesis) and ecosystem respiration (R_{eco}) combine to make the net exchange:

$$NEE = R_{eco} + GPP \tag{1}$$

We use the sign convention that addition of CO_2 to the atmosphere through R_{eco} is positive, carbon uptake by photosynthesis (GPP) is negative, and thus, negative values of NEE indicate net CO_2 uptake from the

Table 1. List of Symbols Used

Symbol	Description	Unit
α	canopy light utilization efficiency	μmol C J^{-1}
β	maximum C uptake rate of the canopy at light saturation	μmol C m^{-2} s^{-1}
c_a	mole fraction of atmospheric CO_2	μmol mol^{-1}
c_{bg}	mole fraction of atmospheric CO_2 at a reference location	μmol mol^{-1}
c_s	change in mole fraction of atmospheric CO_2 resulting from net land-atmosphere exchange	μmol mol^{-1}
$\delta^{13}C$	stable ($^{13}C/^{12}C$) isotope composition (relative to VPDB)	‰
δ_a	$\delta^{13}C$ of atmospheric CO_2	‰
δ_{ab}	$\delta^{13}C$ of gross photosynthesis (atmosphere-biosphere) flux	‰
δ_{ao}	$\delta^{13}C$ of gross ocean uptake (atmosphere-ocean) flux	‰
δ_{ba}	$\delta^{13}C$ of gross biosphere respiration (biosphere-atmosphere) flux	‰
δ_{bg}	$\delta^{13}C$ of atmospheric CO_2 at a reference location	‰
δ_A	$\delta^{13}C$ of ecosystem net photosynthetic assimilation	‰
δ_f	$\delta^{13}C$ of fossil fuel flux	‰
δ_{NEE}	$\delta^{13}C$ of net ecosystem exchange	‰
δ_{oa}	$\delta^{13}C$ of gross ocean release (ocean-atmosphere) flux	‰
δ_R	$\delta^{13}C$ of ecosystem respiration	‰
δ_S	$\delta^{13}C$ of net land-atmosphere exchange	‰
$\delta_{S\text{-day}}$	$\delta^{13}C$ of net land-atmosphere exchange during day	‰
$\delta_{S\text{-night}}$	$\delta^{13}C$ of net land-atmosphere exchange during night	‰
Δ_{canopy}	canopy photosynthetic carbon isotope discrimination	‰
$\Delta^{14}C$	radiocarbon content of organic material (relative to oxalic acid)	‰
D	^{13}C land disequilibrium	‰
ε_{ab}	fractionation of land photosynthesis (atmosphere-biosphere) flux	‰
ε_{ao}	fractionation of ocean uptake (atmosphere-ocean) flux	‰
F_A	ecosystem net photosynthetic assimilation	μmol m^{-2} s^{-1}
F_{ba}	gross biosphere respiration (biosphere-atmosphere) flux	Pg C yr^{-1}
F_f	net global fossil fuel combustion flux	Pg C yr^{-1}
F_l	net global biosphere-atmosphere exchange flux	Pg C yr^{-1}
F_o	net global ocean-atmosphere exchange flux	Pg C yr^{-1}
F_{oa}	gross ocean release (ocean-atmosphere) flux	Pg C yr^{-1}
F_R	ecosystem respiration	μmol m^{-2} s^{-1}
GPP	gross primary productivity (derived from flux partitioning)	μmol m^{-2} s^{-1}
NEE	net ecosystem exchange of CO_2	μmol m^{-2} s^{-1}
NEE*	annual sum of net ecosystem exchange of CO_2	Pg C yr^{-1}
R_{eco}	ecosystem respiration (derived from flux partitioning)	μmol m^{-2} s^{-1}
R_{eco}*	annual sum of ecosystem respiration	Pg C yr^{-1}
t	time	year

atmosphere. A list of symbols is provided in Table 1. Hourly NEE was partitioned into R_{eco} and GPP using two methods, one based on nighttime data and the other on daytime data, each applied to moving 4 day time windows. For all analyses, day and night were defined based on solar calculations and the transition periods (1 h before and after sunrise or sunset) were excluded. Flux partitioning was conducted using the web-based tools maintained by the Max Planck Institute for Biogeochemistry (http://www.bgc-jena.mpg.de/~MDIwork/eddyproc/index.php). Monthly means of the hourly fluxes were calculated for use in our analysis.

1. Reichstein method: The standard Arrhenius-type environmental regression flux partitioning method of *Reichstein et al.* [2005] was applied using regressions of u^* -corrected nighttime NEE versus soil temperature, extrapolated to the daytime, to define R_{eco} and GPP on an hourly basis. This involved a basal respiration rate at 15°C and a temperature sensitivity parameter.

2. Lasslop method: This method was applied via regressions of daytime NEE versus global radiation, adjusted for the role of vapor pressure deficit (VPD), also using an Arrhenius-type formulation for R_{eco} to estimate hourly GPP as described by *Lasslop et al.* [2010]. Only daytime data were used, including for the specification of R_{eco}. This method involved additional parameters of a light response model including canopy light-use efficiency (α, initial slope of light-response curve, using Lasslop's notation), and photosynthetic capacity (β, maximum CO_2 uptake rate under saturating light). The β parameter was adjusted to be an exponential function of VPD [*Lasslop et al.*, 2010].

2.4. Isotope Mixing Relationships

The mixing of CO_2 in air resulting from a combination of a starting point (background, subscript bg) and a net source or sink (subscript s) can be expressed using mass balance for CO_2:

$$c_a + c_{bg} + c_s \qquad (2)$$

and for $^{13}CO_2$ (in δ notation)

$$\delta_a c_a = \delta_{bg} c_{bg} + \delta_s c_s \qquad (3)$$

where c denotes the mole fraction of CO_2, δ its isotopic composition, and subscript a refers to the air. These equations are those used to create the widely used Keeling plot [*Keeling*, 1958; *Pataki et al.*, 2003] but can be combined so that the measured "background" value at a reference (bg) location can be specified [*Miller and Tans*, 2003]:

$$\delta_a c_a - \delta_{bg} c_{bg} = \delta_s (c_a - c_{bg}) \qquad (4)$$

This formulation is useful for comparing observations at one location directly to those made at a reference location. The isotopic composition of land-atmosphere exchange (δ_s) is then derived from the slope of a plot of ($\delta_a c_a - \delta_{bg} c_{bg}$) versus ($c_a - c_{bg}$). *Ballantyne et al.* [2010, 2011] recently used this method to compare NOAA/ESRL flask observations at a variety of sites worldwide to selected reference locations (e.g., the average CO_2 and $\delta^{13}C$ in the marine boundary layer at the latitude of the site, or at the Niwot Ridge tundra site).

We used these equations to calculate δ_s at the forest site on a monthly basis using three separate reference cases (see the supporting information). Selection of an appropriate reference that allowed nonlocal isotopic influences to be removed was found to be important in determining δ_s. For all analyses reported in the main paper, we used the "forest raw" reference.

2.5. Merging Fluxes and Isotopes

The net exchange of CO_2 between a forest and the atmosphere can be also be expressed by CO_2 mass balance as

$$NEE = F_R + F_A \qquad (5)$$

Equation (5) is an alternate formulation of equation (1), where F_R represents the ecosystem respiratory flux and F_A the ecosystem photosynthetic flux. These are conceptually similar to, but not identical to, R_{eco} and GPP. We stress this distinction because the role of foliar respiration in the photosynthetic and respiratory terms in equations (1) and (5) is vague and potentially confounded by the use of different partitioning methods. The associated isotopic mass balance is expressed as

$$\delta_{NEE}(NEE) = \delta_R F_R + \delta_A F_A \qquad (6)$$

where

$$\delta_A = \delta_a - \Delta_{canopy} \qquad (7)$$

Here δ_{NEE}, δ_R, and δ_A are the carbon isotope compositions ($\delta^{13}C$) of the net ecosystem exchange, the respiratory flux, and the photosynthetic flux, respectively. The latter is influenced both by the $\delta^{13}C$ of forest air (δ_a) and the canopy photosynthetic carbon isotope discrimination (Δ_{canopy}).

Equations (5)–(7) were originally derived to use the ^{13}C tracer to partition NEE into F_R and F_A [*Bowling et al.*, 2001, 2003; *Lloyd et al.*, 1996; *Yakir and Wang*, 1996]. For that application, some formulation of Δ_{canopy} was required, and this was estimated based on various combinations of measurements and modeling [e.g., *Bowling et al.*, 2001; *Knohl and Buchmann*, 2005; *Lai et al.*, 2003; *Ogee et al.*, 2003; *Zhang et al.*, 2006; *Zobitz et al.*, 2008]. Traditionally, leaf-level photosynthetic carbon isotope discrimination (Δ) has been studied as a net discrimination [*Farquhar et al.*, 1982], meaning that the leaf photosynthesis and leaf respiration components are included in the net photosynthetic term (F_A) in equations (5) and (6). Hence, the attribution of leaf respiration to particular terms in these equations may be important—this is discussed in section 4.3.
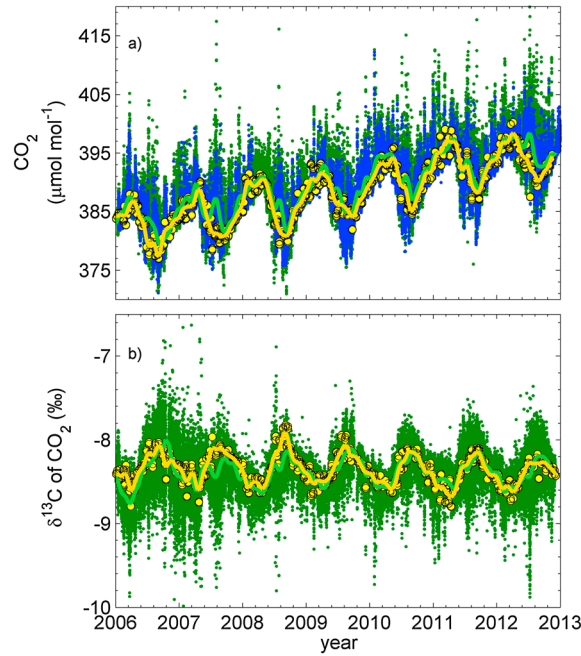
BOWLING ET AL.   5

Figure 1. (a) CO_2 and (b) $\delta^{13}C$ of CO_2 at Niwot Ridge, Colorado, observed over a 7 year period at the alpine tundra and at the subalpine AmeriFlux forest sites. Shown are forest TDL data (green circles) and the curve fit to the forest TDL data (green lines), the tundra flask data (yellow circles) and the curve fit to the tundra flask data (yellow lines), and the tundra AIRCOA data (blue circles). Measurement heights above ground were 21.5 m (forest), 3.5 m (tundra flask), and 5.1 m (tundra AIRCOA). A TDL instrument change in early 2007 improved performance as described by *Schaeffer et al.* [2008a], which explains the higher variability in the early TDL record in Figure 1b).

In the present study, rather than use ^{13}C to calculate F_A and F_R, we instead used the flux partitioning methods above to specify R_{eco} and GPP and combined that information with equations (5)–(7) to examine the ^{13}C land disequilibrium (D):

$$D = \delta_R - \delta_A \qquad (8)$$

The above equations can be combined and modified to reflect the net isotopic composition of exchange during night and day as

$$\delta_{S-day}(\text{NEE}) = \delta_{s-night}R_{eco} + \left(\delta_a - \Delta_{canopy}\right)\text{GPP} \qquad (9)$$

Here $\delta_{S-night}$ represents the isotopic composition of net ecosystem exchange at night, when photosynthesis does not occur, and thus, $\delta_{S-night}$ is the $\delta^{13}C$ of R_{eco}. We assumed that this composition does not change between night and day, which is a common but untested assumption [*Lai et al.*, 2005; *Zhang et al.*, 2006; *Zobitz et al.*, 2008]. The daytime signature of net exchange is given by δ_{S-day} and is influenced by both photosynthetic and respiratory processes. This framework allowed us to use equation (9) to solve for the isotopic composition of the photosynthetic flux (δ_A, see equation (7)) and then evaluate both the ^{13}C land disequilibrium (D) and Δ_{canopy}. This was done on a monthly basis for the 7 year period of record.

2.6. Global Carbon Balance

Implications of our study for the global carbon cycle will be examined in section 4.5 using the global-scale versions of equations (1) and (6):

$$\frac{d}{dt}c_a = F_f + F_l + F_o \qquad (10)$$

$$c_a \frac{d}{dt}\delta_a = (\delta_f - \delta_a)F_f + (\varepsilon_{ao})F_o + (\delta_{oa} - \delta_{ao})F_{oa} + (\varepsilon_{ab})F_l + (\delta_{ba} - \delta_{ab})F_{ba} \qquad (11)$$

These equations and notation are consistent with *Alden et al.* [2010], and derivations for these were provided by *Tans et al.* [1993]. Note that a conversion from μmol mol^{-1} to Pg C yr^{-1} is implicit here. Using our notation for the relevant biosphere (last two) terms, equation (11) becomes

$$c_a \frac{d}{dt}\delta_a = (\delta_f - \delta_a)F_f + (\varepsilon_{ao})F_o + (\delta_{oa} - \delta_{ao})F_{oa} + (\delta_A - \delta_a)(\text{NEE}^*) + (D)(R_{eco}^*) \qquad (12)$$

where NEE* and R_{eco}* denote annual summation of the fluxes (with units of Pg C yr^{-1}).

2.7. Uncertainties and Error Propagation

The standard errors of the monthly means of the fluxes (NEE, GPP, and R_{eco}) and of the $\delta^{13}C$ of atmospheric CO_2 (δ_a, at 11 m height, equation (9)) were used as estimates of uncertainty for each. Isotopic signatures (δ_{S-day}, $\delta_{S-night}$) were assigned uncertainty based on the standard error of the slopes of $\delta_a c_a - \delta_{bg} c_{bg}$ versus ($c_a - c_{bg}$) regressions (ordinary least squares [*Zobitz et al.*, 2006]). For some analyses, all regression results are shown, but for most, only those regressions with $r^2 > 0.85$ (an arbitrary goodness of fit threshold) were used. During winter, and during daytime, reduced variability in CO_2 and $\delta^{13}C$ (see the supporting information) often
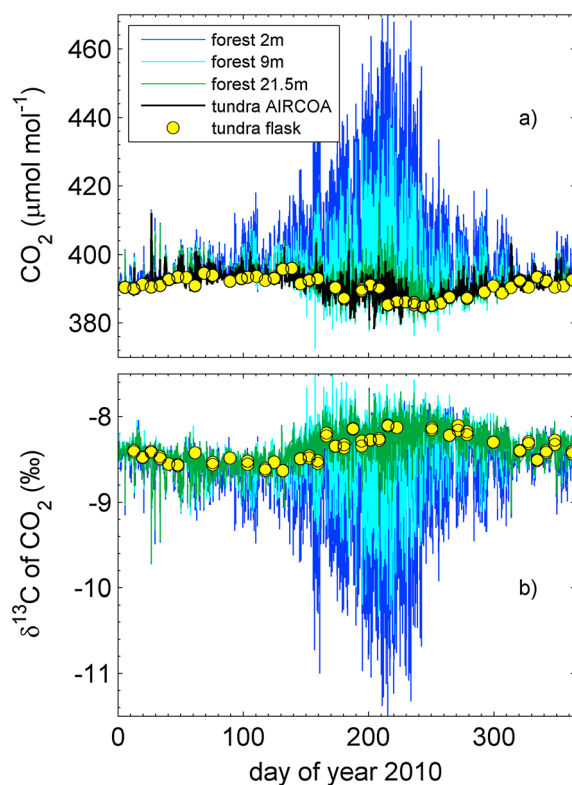
Figure 2. (a) CO_2 and (b) $\delta^{13}C$ of CO_2 at Niwot Ridge during 2010, highlighting the variability observed at the forest site compared to the tundra site. Measurement heights for TDL are indicated, others as in Figure 1.

led to regression results that did not meet this threshold and thus low confidence in our ability to interpret the biological isotope signals of interest. These periods were omitted from analyses in the main paper. Errors were propagated for sums and differences by addition, and for multiplication and division in quadrature.

The isotopic signatures δ_A, δ_R, and D were flux-weighted using GPP, R_{eco}, and NEE, as typically used in global carbon cycle studies (equation (12)), and the flux-weighted means were evaluated with different r^2 threshold criteria on the fits for inclusion in calculating the mean. Propagation of error as above for these cases was not useful due to the large number of calculations in the flux weighting. For these cases, the uncertainty in the flux-weighted means for δ_A, δ_R, and D was estimated using a bootstrap algorithm (subsampling 10,000 times with replacement from the population of monthly parameters, Matlab R2012b, MathWorks, Natick, MA).

2.8. Radiocarbon Composition of Soils and Roots

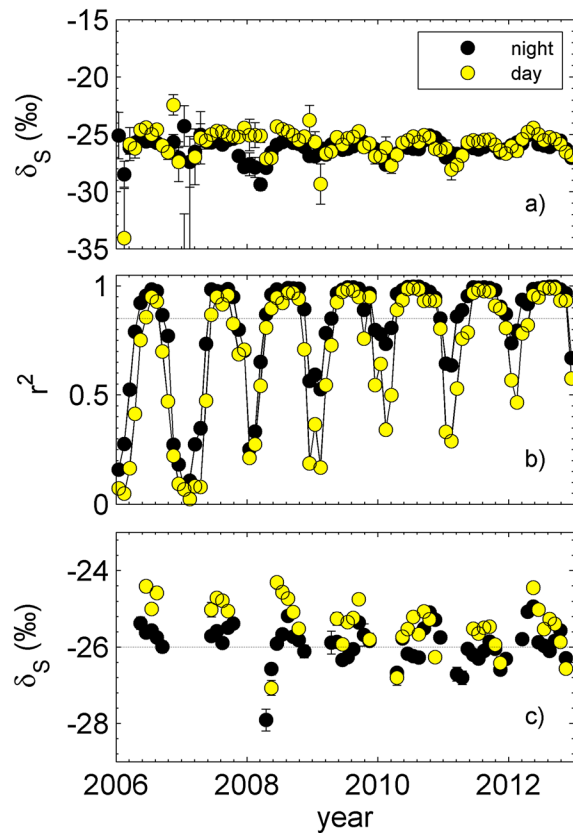Soil cores (5 cm diameter) were collected using a bucket auger in 2006 ($n = 36$ cores). Cores were separated into organic (O) horizon, typically 5–10 cm thick [*Scott-Denton et al.*, 2003], and two mineral (A horizon) soil increments (0–10 and 10–20 cm below the termination of the O horizon). Roots were carefully removed by hand from each sample. Soils and roots were dried to constant mass before analysis. The $\delta^{13}C$ of these samples has been previously reported [*Schaeffer et al.*, 2008b]. Replicate samples were bulked for radiocarbon analysis. Dried mineral soil samples were sieved into size classes (<63, 63–212, and 212–2000 μm). Samples were converted to graphite and analyzed for radiocarbon composition at the Keck Carbon Cycle Accelerator Mass Spectrometry Laboratory at the University of California at Irvine. Results are presented as $\Delta^{14}C$ (relative to oxalic acid) according to protocol for bomb radiocarbon studies [*Trumbore*, 2009]; analytical precision was 1.4–1.8‰. A single pool, steady state model was used to estimate the turnover times of these carbon pools [*Gaudinski et al.*, 2000]. This model cannot reliably determine turnover times for prebomb carbon—we used it as a general indication of the age of some of the carbon pools in the forest. The $\Delta^{14}C$ of atmospheric CO_2 from the Niwot Ridge tundra site for use in this modeling was obtained from *Lehman et al.* [2013].

3. Results

The 7 year records of CO_2 and $\delta^{13}C$ at the tundra and forest sites are shown in Figure 1. The annual means of the flask data at the tundra site in 2012 were 394.5 μmol mol^{-1} and −8.4‰. The secular rise and seasonal cycle of CO_2 were apparent in all records, as was the seasonal cycle in $\delta^{13}C$. The Suess effect (decrease in $\delta^{13}C$) is proceeding at Niwot Ridge at ≈ -0.25‰ decade^{-1} (data not shown), a change too small to discern easily in the 7 years shown in Figure 1. Considerably more variability in CO_2 and $\delta^{13}C$ was observed in the continuous data relative to the flask data at both sites (Figures 1 and 2), with lower CO_2 than the flasks during the summer daytime and higher CO_2 during summer night and in winter. Clear vertical gradients in CO_2 and $\delta^{13}C$ were present at the forest (Figure 2). Variation in both CO_2 and $\delta^{13}C$ was highly reduced in the cold season relative to the summer but still present.

Figure 3. Monthly estimates of δ_S during day (yellow) and night (black) periods calculated separately, using the forest raw reference. Shown are (a) data from all months, (b) the coefficients of determination for each regression, and (c) those data with $r^2 > 0.85$ (horizontal line in Figure 3b). Uncertainties are standard errors of the slope of each regression and are shown for all data but are smaller than the symbols in some cases. Transition periods of 1 h before and after sunrise and sunset were excluded. All forest TDL inlet heights were used with the forest raw reference.

There were clear differences in the δ^{13}C of forest-atmosphere exchange when night and day periods were compared (Figure 3). Lower variation in CO_2 and δ^{13}C in the cold season led to lower regression quality (r^2, Figure 3b). Retention of only those periods with the highest coefficients of determination ($r^2 > 0.85$, $n = 40$ of 80 months remaining) showed that daytime exchange was generally enriched relative to nighttime exchange (Figures 3c and 4) but not always. There was year to year variation in $\delta_{S\text{-night}}$ and $\delta_{S\text{-day}}$ of ≈ 2‰ and larger in some months (Figures 4d and 4e), and seasonal variation as well, particularly for the daytime exchange (e.g., Figures 4a and 4d).

The ecosystem CO_2 fluxes varied strongly over the seasonal cycle and interannually (Figures 4c and 4f). Ecosystem respiration peaked in midsummer at about 5 μmol m^{-2} s^{-1}, and GPP in summer was larger (≈ -12 μmol m^{-2} s^{-1}; Figure 4). The peaks in the fluxes did not usually occur at the same time within the season (data not shown). The flux partitioning methods yielded systematic differences in the derived fluxes of GPP and R_{eco} (Table 2). The GPP and R_{eco} derived using the Lasslop method were 7 and 23% greater in absolute magnitude, respectively, than with the Reichstein method.

The data in Figure 4 were used with equations (7)–(9) to calculate δ_A, Δ_{canopy}, and D, and the results are presented for both partitioning methods in Figure 5. Despite the large and systematic differences in the fluxes GPP and R_{eco} fro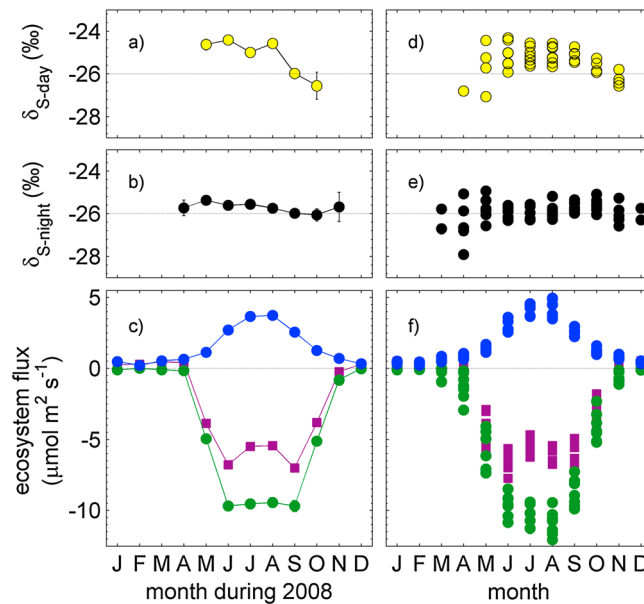m the two approaches (Table 2 and Figures 5d and 5h), the isotopic results were similar. The resulting δ^{13}C of the photosynthetic flux (δ_A, Figures 5a and 5e) was generally more enriched than the respiration flux (Figures 4b and 4e) regardless of partitioning method (not shown, but compare the horizontal lines at -26‰ in these figures). There was a seasonal change in δ_A (Figures 5a and 5e) that was related to a seasonal change in Δ_{canopy} (Figures 5b and 5f). The ^{13}C land disequilibrium also varied seasonally, and for most of the season when GPP and R_{eco} were large, it was negative ($\delta_R < \delta_A$, Figures 5c and 5g).

The seasonal patterns in isotopic signature were qualitatively similar during all 7 years studied (Figure 5). The flux-weighted means of δ_A, δ_R, and D are listed in Table 3. When all data ($n = 84$ months) were considered, the uncertainties in these parameters were large, with some unrealistic values obtained when regressions were poor. Selection of various r^2 thresholds for data quality led to lower uncertainty in the flux-weighted means. The respiratory fluxes (δ_R) were quite consistent at ≈ -26‰ regardless of r^2 threshold or flux partitioning method. The methods were largely consistent in their estimation of flux-weighted δ_A (-25.0 ± 1.7‰), δ_R (-25.9 ± 1.9‰), and D (-0.75 ± 0.21 and -0.87 ± 0.10‰, values for the $r^2 > 0.85$ case). Note that the use of a higher r^2 threshold led to retention of summer months only (Table 3) when biological activity and associated CO_2 and δ^{13}C variation were greatest (Figure 2 and the supporting information).

There was repeated, systematic seasonal variation in Δ_{canopy}, with larger discrimination in the early (May) and late (October) part of the warm season and smaller discrimination in midsummer (Figure 6). This variation was

Figure 4. Annual pattern of monthly (a, d) day and (b, e) night estimates of δ_S from Figure 3 with $r^2 > 0.85$. (c, f) These are compared to monthly mean measured NEE (purple), GPP (green), and R_{eco} (blue) partitioned using the Lasslop method. Shown in the left column are data for 2008, with uncertainties (smaller than the symbol in most cases)—in the right column are data for 2006–2012, with error bars omitted for clarity. Horizontal lines are shown at −26‰ to facilitate comparison of Figures 4a and 4d with 4b and 4e. All forest TDL inlet heights were used with the forest raw reference.

not related to soil moisture (Figure 6a) but was nonlinearly related to vapor pressure deficit of air (Figure 6b). The $\delta^{13}C$ of the respiratory flux varied by $\approx 1.5‰$ (Figures 6c and 6d) and was not related to either soil moisture or VPD. Similar to Δ_{canopy}, the disequilibrium between δ_A and δ_R varied seasonally in relation to VPD.

The radiocarbon composition ($\Delta^{14}C$) of bulk roots, organic, and mineral soil size fractions varied from 151‰ (roots), 123‰ (organic horizon), to 8–73‰ (different mineral size fractions, Table 4). All components had bomb carbon present ($\Delta^{14}C > 0$ indicating post-1950 carbon). The associated turnover times (model results not shown) of these carbon pools from the steady state model were ≈ 17 years (roots), ≈ 12 years (organic horizon), and older (all mineral soils had turnover times of at least 20 years with minor to major contributions from pre-1950).

4. Discussion

This is the first study to attempt to estimate seasonal changes in the ^{13}C land disequilibrium using tower-based observations of biosphere-atmosphere CO_2 exchange. The conceptual approach used here was applied by *Lai et al.* [2005] to examine the $\delta^{13}C$ of daytime NEE in three forests. These researchers used the GlobalView product (http://www.esrl.noaa.gov/gmd/ccgg/globalview) to specify c_{bg} and δ_{bg} in equation (4), combined with twice-weekly daytime flask collections above the vegetation canopy to provide single estimates of $\delta_{S\text{-day}}$ and δ_A for the season. However, resulting uncertainties on δ_A and δ_R were too large to provide information about the ^{13}C land disequilibrium or its seasonality.

Table 2. Results From Ordinary Least Squares Regression of Monthly Mean GPP and R_{eco} Fluxes Derived From Both Partitioning Methods ($n = 84$ Months in All Cases)[a]

Abscissa	Ordinate	Slope	Intercept	r^2
GPP, Reichstein method	GPP, Lasslop method	1.067	−0.093	0.996
R_{eco}, Reichstein method	R_{eco}, Lasslop method	1.229	−0.142	0.979

[a]The slopes are dimensionless, the intercepts are in units of $\mu mol\ CO_2\ m^{-2}\ s^{-1}$.

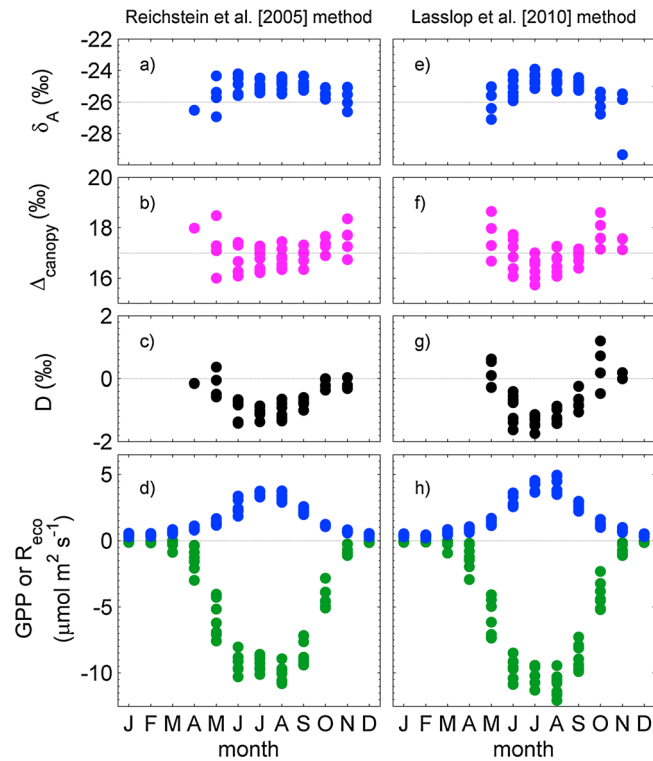**Figure 5.** Derived values of (a, e) δ_A, (b, f) Δ_{canopy}, and the (c, g) ^{13}C disequilibrium (D) associated with each partitioning method (columns). (d, h) The partitioned fluxes GPP (green) and R_{eco} (blue) are shown for each method in the bottom row. Years 2006–2012 are overlapped to shown the overall annual pattern. Horizontal lines are shown at $-26‰$ (for δ_A), 17‰ (Δ_{canopy}), and 0‰ (D) for comparison. All forest TDL inlet heights were used with the forest raw reference. Error bars are omitted for clarity here, but see Figure 6.

Here we have used a 7 year record of land-atmosphere eddy covariance fluxes and the δ^{13}C of net biosphere-atmosphere carbon isotope exchange to quantify D. While δ_S is easily measured at night, it is challenging to obtain this during the daytime because strong atmospheric mixing minimizes the CO_2 and δ^{13}C variation needed to establish the mixing relationships [*Bowling et al.*, 2001; *Griffis et al.*, 2008]. This was possible in our case due to (1) the extensive CO_2 isotope data at the Niwot Ridge forest, which provided thousands of

Table 3. Mean Estimates of δ_A, δ_R, and D Calculated From Each of the Flux Partitioning Methods[a]

r^2 Threshold	n	GPP-Weighted δ_A (‰) Reichstein Method	Lasslop Method	R_{eco}-Weighted δ_R (‰) Reichstein Method	Lasslop Method	NEE-Weighted δ_A (‰) Reichstein Method	Lasslop Method	R_{eco}-Weighted D (‰) Reichstein Method	Lasslop Method
None	84 (Jan–Dec)	−25.0 (2.7)	−25.1 (2.7)	−26.0 (2.2)	−26.0 (2.4)	−26.1 (3.2)	−59.3 (29.4)	−2.8 (1.7)	−52.5 (45.0)
0.75	50 (Mar–Dec)	−25.0 (2.0)	−25.1 (2.1)	−25.9 (2.0)	−25.9 (2.1)	−25.0 (2.2)	−25.1 (2.2)	−0.78 (0.13)	−0.78 (0.28)
0.85	40 (Apr–Nov)	−25.0 (1.7)	−25.0 (1.7)	−25.9 (1.8)	−25.9 (2.0)	−25.0 (1.7)	−25.0 (1.8)	−0.88 (0.10)	−0.75 (0.21)
0.95	17 (May–Sep)	−25.1 (0.5)	−25.1 (0.7)	−26.0 (1.5)	−26.0 (1.8)	−25.1 (0.7)	−25.1 (0.7)	−0.88 (0.10)	−0.91 (0.11)

[a]These parameters have been weighted by GPP, R_{eco}, or NEE as indicated, for comparison to terms in the global carbon cycle (equations (11) and (12), and section 4.5). Shown in the first row are the flux-weighted means for all available data ($n = 84$ months), and in other rows, regressions to determine δ_{S-day} and $\delta_{S-night}$ were excluded if they did not exceed various thresholds of r^2 (first column). Omitting poor regressions led to fewer months represented (number of months n in second column) but generally led to convergence of estimates for δ_A, δ_R, and D for $r^2 > 0.85$ or higher. The actual months represented in each category are shown below the number of months (e.g., Apr–Nov indicates that at least one of the months April through November, inclusive, was retained). Higher thresholds excluded more data, particularly in winter. Uncertainties were estimated using bootstrapping and are shown in parentheses.
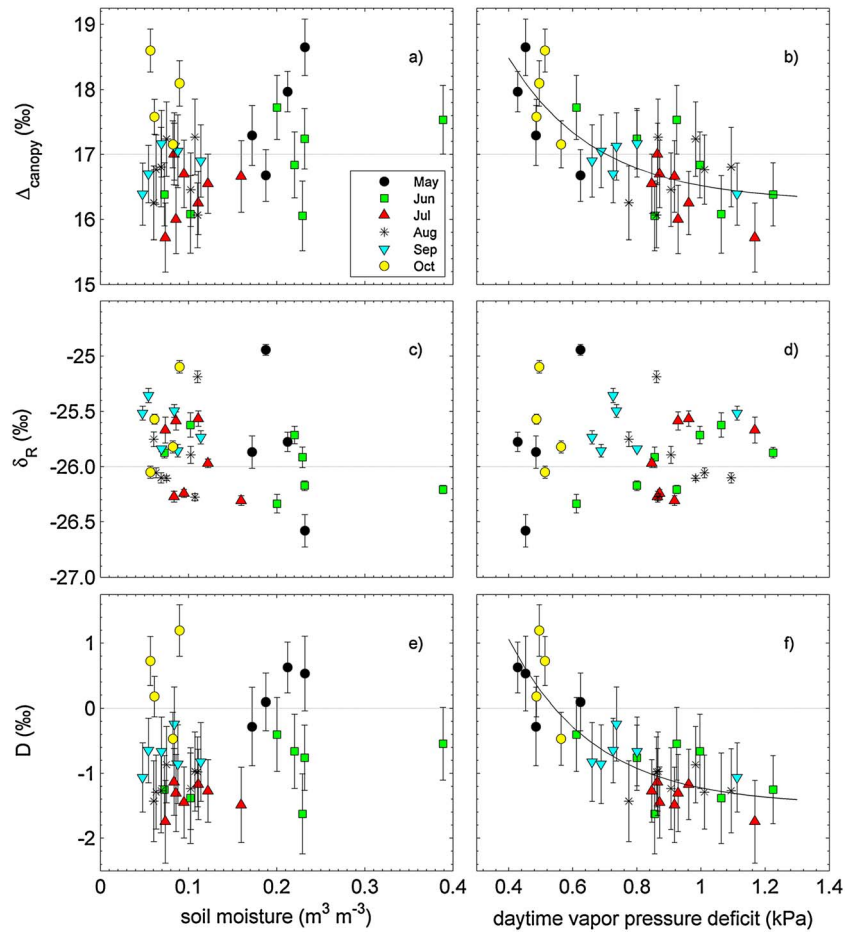
Figure 6. Monthly means of (a, b) ecosystem photosynthetic carbon isotope discrimination, (c, d) $\delta^{13}C$ of ecosystem respiration, and (e, f) the ^{13}C disequilibrium as a function of soil moisture and daytime vapor pressure deficit. Data are shown for particular months with different symbols. The fit lines are $y = 16.27(1 + 058e^{-3.64x})$ and $y = -1.49(1 - 7.69e^{-3.76x})$. Horizontal lines are shown at $-26‰$ (for δ_R), $17‰$ (Δ_{canopy}), and $0‰$ (D) for comparison. All forest TDL inlet heights were used with the forest raw reference.

daytime measurements per month, and (2) the application of a novel mixing approach that used observations above the canopy to remove nonlocal effects on CO_2 and $\delta^{13}C$.

4.1. ^{13}C Land Disequilibrium

Selection of the appropriate reference (specification of c_{bg} and δ_{bg}) was important in removing synoptic influences on the isotopic signatures of land-atmosphere exchange (see the supporting information). This

Table 4. Radiocarbon Composition of Soil and Roots at the Niwot Ridge Forest in 2006[a]

Description	Sampling Depth	Size Class	$\Delta^{14}C$ (‰)
Bulk roots	-	-	151.1
Bulk O horizon	-	-	123.9
A horizon	0–10 cm	212–2000 μm	73.7
A horizon	0–10 cm	63–212 μm	31.3
A horizon	0–10 cm	< 63 μm	23.5
A horizon	10–20 cm	212–2000 μm	62.2
A horizon	10–20 cm	63–212 μm	20.2
A horizon	10–20 cm	< 63 μm	8.0

[a]Organic (O) and mineral (A) horizons were measured, and the A horizon was sampled at two depths and analyzed in three particle size classes. Analytical uncertainty for $\Delta^{14}C$ was 1.4–1.8‰.

step was critical to allow us to focus on local ecological processes at the Niwot Ridge forest. Using the forest raw reference allowed removal of these synoptic influences and robust determination of the $\delta^{13}C$ of the forest photosynthetic flux (δ_A) on a monthly basis over the 7 year study period (Figure 5). Except in May and October, δ_A was more enriched than the respiratory flux (δ_R), leading to negative ^{13}C land disequilibrium (Figure 5); the flux-weighted D was -0.75 to -0.88‰ (using the Lasslop or Reichstein methods, respectively, Table 3). The negative disequilibrium has been observed in other conifer forests. *Wingate et al.* [2010, Figure 6] reported that branch-level observations of the photosynthetic flux were more enriched than ecosystem respiration in a maritime pine forest in summer. *Flanagan et al.* [2012] combined a physiological model of photosynthesis with nocturnal CO_2 isotope measurements to examine δ_A and δ_R in three boreal coniferous forests and similarly found that δ_A was more enriched than δ_R in midsummer. Hence, our observation of negative D is not unique to the Niwot Ridge forest or to our methodological approach.

The negative sign of the disequilibrium contradicts model estimates of D that are based on the residence time of carbon in soil and wood combined with the Suess effect [*Ciais et al.*, 1999; *Fung et al.*, 1997]. Although coarse in spatial resolution, for the mountainous western United States, these models predicted D in the range $+0.25$ to $+0.45$‰. The turnover times calculated from the Niwot Ridge forest radiocarbon data in Table 4 using the steady state model were ≈ 17 years (roots), ≈ 12 years (organic horizon), and longer (+20 years for mineral soil carbon fractions). These turnover times are consistent with contemporary understanding of D, as long as one assumes no long-term trends in photosynthetic fractionation and no post-photosynthetic fractionation. These turnover times are also consistent with studies of carbon stocks and decomposition in subalpine forests [*Bradford et al.*, 2008; *Kueppers and Harte*, 2005; *Kueppers et al.*, 2004], and considering the age of the stand (≈ 110 years), the Suess effect must have been incorporated into these stocks. Despite this, the expected positive disequilibrium was not observed (Figures 5 and 6).

4.2. Seasonality of Δ_{canopy} and D in Response to Environmental Factors

It is well known that photosynthetic carbon isotope discrimination of C_3 plants (including conifers) varies in response to precipitation, soil water content, and atmospheric humidity [*Farquhar et al.*, 1989; *McDowell et al.*, 2010; *Roden and Ehleringer*, 2007; *Warren et al.*, 2001; *Wingate et al.*, 2010]. The isotopic influence of photosynthesis has been shown to propagate through forests within days and can be detected in the $\delta^{13}C$ of forest respiration [*Bowling et al.*, 2002; *Lai et al.*, 2005; *Shim et al.*, 2011] but this is not always true at Niwot Ridge [*Riveros-Iregui et al.*, 2011] and not observed in the present study. We found that monthly Δ_{canopy} varied seasonally from 15.5 to 18.5‰ (Figure 6). This did not appear to be related to soil moisture, which varies seasonally in this forest from fully saturated during snowmelt to a minimum in late summer [*Hu et al.*, 2010b]. There was, however, a nonlinear relationship between monthly Δ_{canopy} and the daytime VPD of air (Figure 6b). This isotopic pattern is consistent with stomatal closure in response to evaporative demand causing decreased photosynthetic discrimination. Stomatal response to atmospheric water vapor is well documented for these tree species [*Andrews et al.*, 2012; *Kaufmann*, 1982] and has a strong seasonal influence on leaf-level gas exchange [*Brodersen et al.*, 2006] and overall forest transpiration rate [*Hu et al.*, 2010b; *Moore et al.*, 2008; *Pataki et al.*, 2000].

Plants that experience seasonal variation in temperature and day length undergo biochemical changes in photosynthetic capacity [*Bauerle et al.*, 2012; *Wilson et al.*, 2001] that seasonally influence leaf-level and ecosystem carbon gain [*Misson et al.*, 2006; *Richardson et al.*, 2009]. The dominant conifers at Niwot Ridge exhibit marked seasonal changes in photosynthetic capacity [*Koh et al.*, 2009], which involve biochemical upregulation of photosynthesis in the spring and downregulation in the fall [*Monson et al.*, 2005; *Zarter et al.*, 2006a, 2006b]. These physiological effects can lead to seasonal changes in photosynthetic discrimination [*Flanagan et al.*, 2012] such as those we have observed (Figures 5 and 6).

The Lasslop flux partitioning method allowed us to calculate canopy-scale photosynthetic capacity (β, section 2.3) and light-use efficiency (α); these varied as expected through the season and were consistent with the leaf-level biochemical studies [*Zarter et al.*, 2006a]. However, neither parameter was correlated with monthly Δ_{canopy} (data not shown). These seasonal changes in photosynthetic capacity were coincident with the seasonal change in VPD in our case (particularly α, data not shown) so their roles are potentially confounded. However, the Lasslop partitioning method uses VPD a priori to calculate β, minimizing this concern. Seasonally varying photosynthetic capacity and stomatal response to VPD probably both contribute to variation in Δ_{canopy} and D over the season (Figures 5 and 6). These data provide strong evidence that forest physiological response to environmental forcing leads to isotopic effects that overshadow the Suess effect.

4.3. Sensitivity to Flux Partitioning and Foliar Respiration

The consistency of our isotope results (δ_A, D) using two flux partitioning methods (Table 3 and Figure 5) provides confidence that our results are not produced by systematic errors in the flux partitioning. Both methods are derived from measured NEE but differ fundamentally in mechanistic formulation and in that the flux partitioning is based on nighttime data [*Reichstein et al.*, 2005] or on daytime data [*Lasslop et al.*, 2010]. The fluxes of GPP and R_{eco} were greater in magnitude using the Lasslop method relative to the Reichstein approach by 7 and 23%, respectively (Table 2), which has been observed at many FLUXNET sites (though the opposite is sometimes true [*Lasslop et al.*, 2010]). Despite this, the flux-weighted estimates of δ_A, δ_R, and D derived from each partitioning method were quite similar when erroneous low r^2 mixing relationships were removed (Table 3).

The role of foliar respiration in equations (5)–(9) deserves comment. Studies which use a c_i/c_a type model for net photosynthetic discrimination (Δ_{canopy}) [*Bowling et al.*, 2001; *Ogee et al.*, 2003] will assign leaf respiration to the F_A term. This is not an issue in our case since we solved for δ_A and Δ_{canopy} using equations (8) and (9) and hence were not dependent on a c_i/c_a framework. The Reichstein method involves regression of nocturnal NEE with temperature to determine R_{eco}, so foliar respiration is accounted for in the R_{eco} term. The Lasslop method uses a light-response curve formulation for photosynthesis that is modified to account for influence of VPD on GPP [*Lasslop et al.*, 2010]. This is more physiologically realistic but is still an oversimplification of the processes involved. There is conflicting evidence from plant physiological studies that leaf mitochondrial respiration is reduced in the light relative to the dark [*Atkin et al.*, 1998; *Brooks and Farquhar*, 1985; *Loreto et al.*, 2001; *Tcherkez et al.*, 2008]. If true, the Lasslop method may reflect the daytime respiratory reduction since it is based on daytime NEE, but note that the R_{eco} and GPP fluxes were highest using this method (Table 2). The similarity of our results for δ_A, δ_R, and D using the Reichstein and Lasslop methods (Table 3) is encouraging and suggests our isotopic results are not sensitive to these complications.

4.4. Resolution With the Suess Effect

Clearly our working hypothesis, that the Suess effect is the dominant factor influencing the isotopic composition of biosphere-atmosphere CO_2 exchange fluxes, is too simplistic. There are at least four possible reasons why the disequilibrium we have obtained conflicts with expectations from the Suess effect. First, the stomatal response to humidity almost certainly leads to changes in Δ_{canopy} as discussed above. This may be an effect that occurs only in water-limited forests. Since the stomatal response affects both the carbon and water cycles, it should be detectable in water use efficiency derived from flux tower observations [*Beer et al.*, 2009; *Brümmer et al.*, 2012; *Ponton et al.*, 2006]. Such an analysis is beyond the scope of the present paper but could provide an extension to the hundreds of other flux tower sites that do not include CO_2 isotope observations, to evaluate whether the ^{13}C land disequilibrium might behave similarly elsewhere. Note that *Flanagan et al.* [2012] concluded for boreal forests that seasonal variation in δ_A was driven by seasonal variation in photosynthetic capacity related to temperature and not VPD, so the importance of these processes is likely to differ across biomes.

Second, as CO_2 has risen over the last 250+ years, there have been widespread changes in photosynthesis, and as a result, the water use efficiency (derived from δ^{13}C of tree rings) of C_3 plants has increased [*Feng*, 1999; *Franks et al.*, 2013; *Loader et al.*, 2011; *Yakir*, 2011]. Change in water use efficiency has been independently confirmed over the last two decades with flux tower observations [*Keenan et al.*, 2013]. This change is evidence that photosynthetic discrimination has decreased since the Industrial Revolution. The direction of change offsets the change in δ^{13}C of atmospheric CO_2, which would tend to diminish the Suess effect. Thus, the isotopic composition of respired CO_2 in forested ecosystems incorporates processes that have competing isotope effects.

Third, the climate of Colorado has changed in recent decades. This region has experienced lower snowfall and earlier snowmelt and higher air temperature than in the past [*Clow*, 2010]. Mean annual air temperature at Niwot Ridge has increased 1.0–1.3°C decade^{-1} since the early 1980s [*Clow*, 2010; *Mitton and Ferrenberg*, 2012]. Higher temperature may lead to higher VPD and lower discrimination on average. Generally, the patterns in disequilibrium we have observed may reflect a recent but sustained change in photosynthetic discrimination in response to climate and rising CO_2.

Finally, there are a wide variety of carbon isotope changes within an ecosystem (collectively called post-photosynthetic fractionation) that occur following photosynthesis. Plant tissues are constructed from the

products of photosynthesis and carbon is differentially allocated to different plant organs, so $\delta^{13}C$ of plant metabolites and tissues differs in systematic ways [*Bowling et al.*, 2008; *Brüggemann et al.*, 2011; *Tcherkez et al.*, 2011]. As carbon is transferred from plant pools to other ecosystem pools through herbivory, root exudation, and mortality, there are additional fractionations but most of them are poorly understood. These effects all combine to influence the $\delta^{13}C$ of leaf, root, and heterotrophic respiration in complex ways [*Barbour et al.*, 2011; *Brüggemann et al.*, 2011; *Werner and Gessler*, 2011; *Zhu and Cheng*, 2011]. In earlier studies at the Niwot Ridge forest, we found that nocturnal δ_R on a nightly basis tended to be more enriched within the vegetation canopy relative to near the ground [*Bowling et al.*, 2005; *Riveros-Iregui et al.*, 2011]. This is qualitatively consistent with plant-scale observations of relatively enriched foliar respiration [*Bowling et al.*, 2008; *Wingate et al.*, 2010] and relatively depleted root respiration [*Ghashghaie and Badeck*, 2014; *Schnyder and Lattanzi*, 2005; *Zhu and Cheng*, 2011]. These results complicate the simple conceptual model we have used (equations (5)–(9)) and suggest that more complex biophysical models [*Baldocchi and Bowling*, 2003; *Flanagan et al.*, 2012; *Wingate et al.*, 2010] combined with flux and isotopic flux observations from different ecosystem pools are likely the best way to investigate the isotopic composition of the photosynthesis and respiratory fluxes. Moreover, the differences between $\delta^{13}C$ of foliar and root respiration point to the necessity of measuring $\delta^{13}C$ of ecosystem respiration in order to avoid bias in calculating *D*. For example, if δ_R in this study were biased toward the more depleted respiration observed at the lower inlets, this would lead to a larger negative bias in *D*.

It is possible that our conclusions about disequilibrium may be biased to the warm season because the isotopic mixing relationships we used require variation in CO_2 and $\delta^{13}C$ which is minimal in winter (Figure 2 and the supporting information). It is possible that respiration during the winter might provide an isotopic balance to the negative disequilibrium we have observed in the warm season. However, the similarity of $\delta^{13}C$ of respiration derived in the present paper with that from under snow observations (supporting information) combined with low R_{eco} in winter (Figures 5d and 5h) provides confidence that there is no seasonal bias.

Conservation of mass requires that disequilibrium between ^{13}C-enriched photosynthetic and ^{13}C-depleted respiratory fluxes be balanced by accumulation of the heavy ^{13}C isotope within the ecosystem. It is important to keep in mind that different carbon pools have different residence times and different isotopic compositions (see Figure 5 and related discussion in *Bowling et al.* [2008]), and together, these pools and the biosphere-atmosphere exchange fluxes must be balanced. Wood (boles, branches, and roots) tends to be enriched in ^{13}C relative to leaves by 1–2‰ [*Bowling et al.*, 2008; *Leavitt and Long*, 1982]. Soil organic matter becomes enriched over time and with depth [*Ehleringer et al.*, 2000], and this is true at Niwot Ridge [*Schaeffer et al.*, 2008b]. There is ≈ 125 Mg C ha^{-1} in standing wood and coarse woody debris, 75 Mg C ha^{-1} in the organic horizon (above the mineral soil), and ≈ 50 Mg C ha^{-1} in the mineral soil at the Niwot Ridge forest [*Bradford et al.*, 2008]. The wood and soil pools have residence times of decades to centuries (Table 4). It is possible that there is enough ^{13}C in these carbon pools to account for the flux imbalance in δ_A and δ_R.

4.5. Implications for the Global Carbon Cycle

It is unlikely that our results are representative of all terrestrial biomes, as they imply a global carbon balance that is in disagreement with current understanding of ocean-atmosphere exchange. Assume the following values for quantities in equations (10) and (11): CO_2 increase rate of 2 μmol mol^{-1} yr^{-1}, decrease in δ_a of -0.025‰ yr^{-1}, $c_a = 395$ μmol mol^{-1} (Figure 1), $\delta_a = -8.4$‰ (Figure 1), $F_f = +8$ Pg C yr^{-1}, $\delta_f = -29$‰, $\varepsilon_{ao} = -2$‰, $\varepsilon_{ab} = -16$‰, $F_{ba} = +50$ Pg C yr^{-1}, $F_{oa} = +70$ Pg C yr^{-1}, ocean disequilibrium $(\delta_{oa} - \delta_{ao}) = +0.6$‰, and the land disequilibrium matches our finding $(\delta_{ba} - \delta_{ab}) = -0.8$‰ (Table 3). If we then solve for F_l and F_o, we find a net terrestrial uptake of -10 Pg C yr^{-1} and a net ocean source of $+6$ Pg C yr^{-1}. The latter conflicts with several independent lines of evidence using atmospheric O_2/N_2 ratios [*Manning and Keeling*, 2006], oceanic pCO_2 [*Takahashi et al.*, 2009], and long-term ocean inorganic carbon measurements [*Sabine et al.*, 2004], which all point to global ocean uptake fluxes between -1 and -3 Pg C yr^{-1}.

In our case, the total (ocean + land) disequilibrium flux in equation (11) was $(\delta_{oa} - \delta_{ao}) F_{oa} + (\delta_{ba} - \delta_{ab}) F_{ba} = +2$ Pg C ‰ yr^{-1}. In contrast, *Alden et al.* [2010] found a total disequilibrium flux of ~115 Pg C ‰ yr^{-1} in 2009 was required to close the CO_2 and $\delta^{13}C$ budgets given global ocean flux estimates of ~ -2 Pg C yr^{-1}. Using their disequilibrium flux of 115 Pg C ‰ yr^{-1} with our values above leads to F_o and F_l of -1.9 Pg C yr^{-1} and -1.8 Pg C yr^{-1}, respectively, which is in agreement with the ocean studies. If our finding of negative disequilibrium at Niwot Ridge is correct, these results collectively imply that there must be a very different isotopic pattern of exchange somewhere else in the terrestrial biosphere or in the oceans.

The research presented here demonstrates that intensive CO_2 isotope observations can reveal processes that challenge conventional wisdom about carbon exchange between the biosphere and atmosphere and the isotopic signature it contains. There are several areas where future research could be prioritized. First, there are now many flux tower sites around the world with intensive observations of δ^{13}C of CO_2 [e.g., *Flanagan et al.*, 2012; *Lai et al.*, 2005; *Torn et al.*, 2011; *Wingate et al.*, 2010]. Existing data sets in a variety of C_3 biomes can be analyzed to determine if the negative disequilibrium is a spatially coherent phenomenon. Special attention to high-precipitation biomes in the tropics and temperate latitudes would help to determine if water limitation is a major factor. Second, studies of the δ^{13}C of photosynthetic and respiratory fluxes from individual ecosystem components [*Wingate et al.*, 2010] could be expanded to a variety of biomes. Third, advancements in isotopic pulse labeling and measurement have allowed substantial progress in understanding plant and ecosystem carbon allocation and fluxes, and continued efforts will help reveal the processes at work [*Epron et al.*, 2012; *Hogberg et al.*, 2008]. More sophisticated isotope-enabled models of carbon assimilation, at scales from the flux tower [*Baldocchi and Bowling*, 2003; *Flanagan et al.*, 2012] and larger [*Raczka et al.*, 2013; *van der Velde et al.*, 2013] could be developed and applied to evaluate possible mechanisms involved. Isotope measurements of CO_2 are a fundamental component of the growing global integrated carbon observing system and will present an excellent opportunity for testing whether the current generation of Earth System Models can accurately simulate the physical and ecological mechanisms controlling biosphere-atmosphere carbon exchange.

In conclusion, we have observed a difference in the isotopic composition of ecosystem photosynthesis and respiration fluxes in a subalpine forest in Colorado, which was repeated over 7 years. When flux weighted, the disequilibrium was negative ($\delta_A > \delta_R$) which is opposite in sign to expectations based on the ^{13}C Suess effect alone. The disequilibrium varied seasonally because the δ^{13}C of the photosynthetic flux changed. This was caused by stomatal response to evaporative demand and possibly also by changing photosynthetic capacity as trees responded to seasonal change in temperature. The conflict with Suess effect expectations may be explained by long-term changes in photosynthetic discrimination as CO_2 and/or temperature have risen, by post-photosynthetic fractionation events of unknown mechanism, or a combination of these.

References

Alden, C. B., J. B. Miller, and J. W. C. White (2010), Can bottom-up ocean CO_2 fluxes be reconciled with atmospheric ^{13}C observations?, *Tellus, Ser. B*, 62(5), 369–388.

Andrews, S. F., L. B. Flanagan, E. J. Sharp, and T. Cai (2012), Variation in water potential, hydraulic characteristics and water source use in montane Douglas-fir and lodgepole pine trees in southwestern Alberta and consequences for seasonal changes in photosynthetic capacity, *Tree Physiol.*, 32, 146–160.

Atkin, O. K., J. R. Evans, and K. Siebke (1998), Relationship between the inhibition of leaf respiration by light and enhancement of leaf dark respiration following light treatment, *Aust. J. Plant Physiol.*, 25(4), 437–443.

Baldocchi, D. D., and D. R. Bowling (2003), Modelling the discrimination of $^{13}CO_2$ above and within a temperate broad-leaved forest canopy on hourly to seasonal time scales, *Plant Cell Environ.*, 26(2), 231–244.

Baldocchi, D. D., et al. (2001), FLUXNET: A new tool to study the temporal and spatial variability of ecosystem-scale carbon dioxide, water vapor, and energy flux densities, *Bull. Am. Meteorol. Soc.*, 82(11), 2415–2434.

Ballantyne, A. P., J. B. Miller, and P. P. Tans (2010), Apparent seasonal cycle in isotopic discrimination of carbon in the atmosphere and biosphere due to vapor pressure deficit, *Global Biogeochem. Cycles*, 24, GB3018, doi:10.1029/2009GB003623.

Ballantyne, A. P., J. B. Miller, I. T. Baker, P. P. Tans, and J. W. C. White (2011), Novel applications of carbon isotopes in atmospheric CO_2: What can atmospheric measurements teach us about processes in the biosphere?, *Biogeosciences*, 8(10), 3093–3106.

Ballantyne, A. P., C. B. Alden, J. B. Miller, P. P. Tans, and J. W. C. White (2012), Increase in observed net carbon dioxide uptake by land and oceans during the past 50 years, *Nature*, 488(7409), 70–72.

Barbour, M. M., J. E. Hunt, N. Kodama, J. Laubach, T. M. McSeveny, G. N. D. Rogers, G. Tcherkez, and L. Wingate (2011), Rapid changes in δ^{13}C of ecosystem-respired CO_2 after sunset are consistent with transient ^{13}C enrichment of leaf respired CO_2, *New Phytol.*, 190, 990–1002, doi:10.1111/j.1469-8137.2010.03635.x.

Bauerle, W. L., R. Oren, D. A. Way, S. S. Qian, P. C. Stoy, P. E. Thornton, J. D. Bowden, F. M. Hoffman, and R. F. Reynolds (2012), Photoperiodic regulation of the seasonal pattern of photosynthetic capacity and the implications for carbon cycling, *Proc. Natl. Acad. Sci. U.S.A.*, 109(22), 8612–8617.

Beer, C., et al. (2009), Temporal and among-site variability of inherent water use efficiency at the ecosystem level, *Global Biogeochem. Cycles*, 23, GB2018, doi:10.1029/2008GB003233.

Beer, C., et al. (2010), Terrestrial gross carbon dioxide uptake: Global distribution and covariation with climate, *Science*, 329(5993), 834–838.

Bowling, D. R., P. P. Tans, and R. K. Monson (2001), Partitioning net ecosystem carbon exchange with isotopic fluxes of CO_2, *Global Change Biol.*, 7(2), 127–145.

Bowling, D. R., N. G. McDowell, B. J. Bond, B. E. Law, and J. R. Ehleringer (2002), ^{13}C content of ecosystem respiration is linked to precipitation and vapor pressure deficit, *Oecologia*, 131(1), 113–124.

Bowling, D. R., D. E. Pataki, and J. R. Ehleringer (2003), Critical evaluation of micrometeorological methods for measuring ecosystem-atmosphere isotopic exchange of CO_2, *Agric. For. Meteorol.*, 116(3–4), 159–179.

Bowling, D. R., S. P. Burns, T. J. Conway, R. K. Monson, and J. W. C. White (2005), Extensive observations of CO_2 carbon isotope content in and above a high-elevation subalpine forest, *Global Biogeochem. Cycles*, 19, GB3023, doi:10.1029/2004GB002394.

Bowling, D. R., D. E. Pataki, and J. T. Randerson (2008), Carbon isotopes in terrestrial ecosystem pools and CO_2 fluxes, *New Phytol.*, *178*, 24–40, doi:10.1111/j.1469-8137.2007.02342.x.

Bradford, J. B., R. A. Birdsey, L. A. Joyce, and M. G. Ryan (2008), Tree age, disturbance history, and carbon stocks and fluxes in subalpine Rocky Mountain forests, *Global Change Biol.*, *14*(12), 2882–2897.

Brodersen, C. R., M. J. Germino, and W. K. Smith (2006), Photosynthesis during an episodic drought in *Abies lasiocarpa* and *Picea engelmannii* across an alpine treeline, *Arct. Antarct. Alp. Res.*, *38*(1), 34–41.

Brooks, A., and G. D. Farquhar (1985), Effect of temperature on the CO_2/O_2 specificity of ribulose-1,5-bisphosphate carboxylase/oxygenase and the rate of respiration in the light—Estimates from gas-exchange measurements on spinach, *Planta*, *165*(3), 397–406.

Brooks, B. G. J., A. R. Desai, B. B. Stephens, D. R. Bowling, S. P. Burns, A. S. Watt, S. L. Heck, and C. Sweeney (2012), Assessing filtering of mountaintop CO_2 mole fractions for application to inverse models of biosphere-atmosphere carbon exchange, *Atmos. Chem. Phys.*, *12*, 2099–2115.

Brüggemann, N., et al. (2011), Carbon allocation and carbon isotope fluxes in the plant-soil-atmosphere continuum: A review, *Biogeosciences*, *8*(11), 3457–3489.

Brümmer, C., et al. (2012), How climate and vegetation type influence evapotranspiration and water use efficiency in Canadian forest, peatland and grassland ecosystems, *Agric. For. Meteorol.*, *153*, 14–30.

Bush, S. E., D. E. Pataki, and J. R. Ehleringer (2007), Sources of variation in $\delta^{13}C$ of fossil fuel emissions in Salt Lake City, USA, *Appl. Geochem.*, *22*(4), 715–723.

Cernusak, L. A., N. Ubierna, K. Winter, J. A. M. Holtum, J. D. Marshall, and G. D. Farquhar (2013), Environmental and physiological determinants of carbon isotope discrimination in terrestrial plants, *New Phytol.*, *200*(4), 950–965.

Ciais, P., P. P. Tans, J. W. C. White, M. Trolier, R. J. Francey, J. A. Berry, D. R. Randall, P. J. Sellers, J. G. Collatz, and D. S. Schimel (1995), Partitioning of ocean and land uptake of CO_2 as inferred by $d^{13}C$ measurements from the NOAA Climate Monitoring and Diagnostics Laboratory Global Air Sampling Network, *J. Geophys. Res.*, *100*(D3), 5051–5070.

Ciais, P., P. Friedlingstein, D. S. Schimel, and P. P. Tans (1999), A global calculation of the $\delta^{13}C$ of soil respired carbon: Implications for the biospheric uptake of anthropogenic CO_2, *Global Biogeochem. Cycles*, *13*(2), 519–530.

Clow, D. W. (2010), Changes in the timing of snowmelt and streamflow in Colorado: A response to recent warming, *J. Clim.*, *23*(9), 2293–2306.

Conway, T. J., P. P. Tans, L. S. Waterman, and K. W. Thoning (1994), Evidence for interannual variability of the carbon cycle from the National Oceanic and Atmospheric Administration/Climate Monitoring and Diagnostics Laboratory Global Air Sampling Network, *J. Geophys. Res.*, *99*(D11), 22,831–22,855.

Desai, A. R., et al. (2011), Seasonal pattern of regional carbon balance in the central Rocky Mountains from surface and airborne measurements, *J. Geophys. Res.*, *116*, G04009, doi:10.1029/2011JG001655.

Ehleringer, J. R., N. Buchmann, and L. B. Flanagan (2000), Carbon isotope ratios in belowground carbon cycle processes, *Ecol. Appl.*, *10*(2), 412–422.

Epron, D., et al. (2012), Pulse-labelling trees to study carbon allocation dynamics: A review of methods, current knowledge and future prospects, *Tree Physiol.*, *32*(6), 776–798.

Falkowski, P., et al. (2000), The global carbon cycle: A test of our knowledge of earth as a system, *Science*, *290*(5490), 291–296.

Farquhar, G. D., M. H. O'Leary, and J. A. Berry (1982), On the relationship between carbon isotope discrimination and the intercellular carbon dioxide concentration in leaves, *Aust. J. Plant Physiol.*, *9*(2), 121–137.

Farquhar, G. D., J. R. Ehleringer, and K. T. Hubick (1989), Carbon isotope discrimination and photosynthesis, *Annu. Rev. Plant Physiol. Plant Mol. Biol.*, *40*, 503–537.

Feng, X. (1999), Trends in intrinsic water-use efficiency of natural trees for the past 100–200 years: A response to atmospheric CO_2 concentration, *Geochim. Cosmochim. Acta*, *63*(13–14), 1891–1903.

Flanagan, L. B., T. Cai, T. A. Black, A. G. Barr, J. H. McCaughey, and H. A. Margolis (2012), Measuring and modeling ecosystem photosynthesis and the carbon isotope composition of ecosystem-respired CO_2 in three boreal coniferous forests, *Agric. For. Meteorol.*, *153*, 165–176.

Francey, R. J., C. E. Allison, D. M. Etheridge, C. M. Trudinger, I. G. Enting, M. Leuenberger, R. L. Langenfelds, E. Michel, and L. P. Steele (1999), A 1000-year high precision record of $d^{13}C$ in atmospheric CO_2, *Tellus, Ser. B*, *51*, 170–193.

Frank, D., A. Pontes, and K. McFarlane (2012), Controls on soil organic carbon stocks and turnover among North American ecosystems, *Ecosystems*, *15*(4), 604–615.

Franks, P. J., et al. (2013), Sensitivity of plants to changing atmospheric CO_2 concentration: From the geological past to the next century, *New Phytol.*, *197*(4), 1077–1094.

Friedlingstein, P., et al. (2006), Climate-carbon cycle feedback analysis: Results from the C^4MIP model intercomparison, *J. Clim.*, *19*(14), 3337–3353.

Fung, I., et al. (1997), Carbon 13 exchanges between the atmosphere and biosphere, *Global Biogeochem. Cycles*, *11*(4), 507–533.

Gaudinski, J. B., S. E. Trumbore, E. A. Davidson, and S. H. Zheng (2000), Soil carbon cycling in a temperate forest: Radiocarbon-based estimates of residence times, sequestration rates and partitioning of fluxes, *Biogeochemistry*, *51*(1), 33–69.

Ghashghaie, J., and F. W. Badeck (2014), Opposite carbon isotope discrimination during dark respiration in leaves versus roots—A review, *New Phytol.*, *201*, 751–769.

Greenland, D. (1989), The Climate of Niwot Ridge, Front Range, Colorado, U.S.A, *Arct. Alp. Res.*, *21*(4), 380–391.

Griffis, T. J., S. D. Sargent, J. M. Baker, X. Lee, B. D. Tanner, J. Greene, E. Swiatek, and K. Billmark (2008), Direct measurement of biosphere-atmosphere isotopic CO_2 exchange using the eddy covariance technique, *J. Geophys. Res.*, *113*, D08304, doi:10.1029/2007JD009297.

Hemming, D., et al. (2005), Pan-European $\delta^{13}C$ values of air and organic matter from forest ecosystems, *Global Change Biol.*, *11*, 1065–1093.

Hogberg, P., et al. (2008), High temporal resolution tracing of photosynthate carbon from the tree canopy to forest soil microorganisms, *New Phytol.*, *177*(1), 220–228.

Hu, J., D. J. P. Moore, S. P. Burns, and R. K. Monson (2010a), Longer growing seasons lead to less carbon sequestration by a subalpine forest, *Global Change Biol.*, *16*, 771–783, doi:10.1111/j.1365-2486.2009.01967.x.

Hu, J., D. J. P. Moore, D. A. Riveros-Iregui, S. P. Burns, and R. K. Monson (2010b), Modeling whole-tree carbon assimilation rate using observed transpiration rates and needle sugar carbon isotope ratios, *New Phytol.*, *185*(4), 1000–1015.

Joos, F., and M. Bruno (1998), Long-term variability of the terrestrial and oceanic carbon sinks and the budgets of the carbon isotopes ^{13}C and ^{14}C, *Global Biogeochem. Cycles*, *12*(2), 277–295.

Kaufmann, M. (1982), Leaf conductance as a function of photosynthetic photon flux density and absolute humidity difference from leaf to air, *Plant Physiol.*, *69*, 1018–1022.

Keeling, C. D. (1958), The concentration and isotopic abundances of atmospheric carbon dioxide in rural areas, *Geochim. Cosmochim. Acta*, *13*(4), 322–334.

Keeling, C. D. (1979), The Suess effect: [13]Carbon-[14]Carbon interrelations, *Environ. Int.*, *2*(4–6), 229–300.

Keenan, T. F., D. Y. Hollinger, G. Bohrer, D. Dragoni, J. W. Munger, H. P. Schmid, and A. D. Richardson (2013), Increase in forest water-use efficiency as atmospheric carbon dioxide concentrations rise, *Nature*, *499*(7458), 324–327.

Knohl, A., and N. Buchmann (2005), Partitioning the net CO_2 flux of a deciduous forest into respiration and assimilation using stable carbon isotopes, *Global Biogeochem. Cycles*, *19*, GB4008, doi:10.1029/2004GB002301.

Knowles, J. F., P. D. Blanken, M. W. Williams, and K. M. Chowanski (2012), Energy and surface moisture seasonally limit evaporation and sublimation from snow-free alpine tundra, *Agric. For. Meteorol.*, *157*, 106–115.

Koh, S. C., B. Demmig-Adams, and W. W. Adams (2009), Novel patterns of seasonal photosynthetic acclimation, including interspecific differences, in conifers over an altitudinal gradient, *Arct. Antarct. Alp. Res.*, *41*(3), 317–322.

Kueppers, L. M., and J. Harte (2005), Subalpine forest carbon cycling: Short- and long-term influence of climate and species, *Ecol. Appl.*, *15*(6), 1984–1999.

Kueppers, L. M., J. Southon, P. Baer, and J. Harte (2004), Dead wood biomass and turnover time, measured by radiocarbon, along a subalpine elevation gradient, *Oecologia*, *141*(4), 641–651.

Lai, C.-T., A. J. Schauer, C. Owensby, J. M. Ham, and J. R. Ehleringer (2003), Isotopic air sampling in a tallgrass prairie to partition net ecosystem CO_2 exchange, *J. Geophys. Res.*, *108*(D18), 4566, doi:10.1029/2002JD003369.

Lai, C.-T., J. R. Ehleringer, A. J. Schauer, P. P. Tans, D. Y. Hollinger, K. T. Paw U, J. W. Munger, and S. C. Wofsy (2005), Canopy-scale δ^{13}C of photosynthetic and respiratory CO_2 fluxes: Observations in forest biomes across the United States, *Global Change Biol.*, *11*(4), 633–643.

Lasslop, G., M. Reichstein, D. Papale, A. Richardson, A. Arneth, A. Barr, P. Stoy, and G. Wohlfahrt (2010), Separation of net ecosystem exchange into assimilation and respiration using a light response curve approach: Critical issues and global evaluation, *Global Change Biol.*, *16*, 187–208.

Le Quere, C., et al. (2009), Trends in the sources and sinks of carbon dioxide, *Nat. Geosci.*, *2*(12), 831–836.

Leavitt, S., and A. Long (1982), Evidence for ^{13}C/^{12}C fractionation between tree leaves and wood, *Nature*, *298*, 742–744.

Lehman, S. J., et al. (2013), Allocation of terrestrial carbon sources using $^{14}CO_2$: Methods, measurement, and modeling, *Radiocarbon*, *55*(2–3), 1484–1495.

Levin, I., S. Hammer, B. Kromer, and F. Meinhardt (2008), Radiocarbon observations in atmospheric CO_2: Determining fossil fuel CO_2 over Europe using Jungfraujoch observations as background, *Sci. Total Environ.*, *391*(2–3), 211–216.

Lloyd, J., et al. (1996), Vegetation effects on the isotopic composition of atmospheric CO_2 at local and regional scales: Theoretical aspects and a comparison between rain forest in Amazonia and a boreal forest in Siberia, *Aust. J. Plant Physiol.*, *23*, 371–399.

Loader, N. J., R. P. D. Walsh, I. Robertson, K. Bidin, R. C. Ong, G. Reynolds, D. McCarroll, M. Gagen, and G. H. F. Young (2011), Recent trends in the intrinsic water-use efficiency of ringless rainforest trees in Borneo, *Philos. Trans. R. Soc. B*, *366*(1582), 3330–3339.

Loreto, F., V. Velikova, and G. D. Marco (2001), Respiration in the light measured by $^{12}CO_2$ emission in $^{13}CO_2$ atmosphere in maize leaves, *Aust. J. Plant Physiol.*, *28*, 1103–1108.

Mahecha, M. D., et al. (2010), Global convergence in the temperature sensitivity of respiration at ecosystem level, *Science*, *329*(5993), 838–840.

Manning, A. C., and R. F. Keeling (2006), Global oceanic and land biotic carbon sinks from the Scripps atmospheric oxygen flask sampling network, *Tellus, Ser. B*, *58*(2), 95–116.

McDowell, N. G., C. D. Allen, and L. Marshall (2010), Growth, carbon-isotope discrimination, and drought-associated mortality across a *Pinus ponderosa* elevational transect, *Global Change Biol.*, *16*(1), 399–415.

Miller, J. B., and P. P. Tans (2003), Calculating isotopic fractionation from atmospheric measurements at various scales, *Tellus, Ser. B*, *55*, 207–214.

Misson, L., K. Tu, R. A. Boniello, and A. H. Goldstein (2006), Seasonally of photosynthetic parameters in a multi-specific and vertically complex forest ecosystem in the Sierra Nevada of California, *Tree Physiol.*, *26*(6), 729–741.

Mitton, J. B., and S. M. Ferrenberg (2012), Mountain pine beetle develops an unprecedented summer generation in response to climate warming, *Am. Nat.*, *179*(5), 1–9.

Monson, R. K., A. A. Turnipseed, J. P. Sparks, P. C. Harley, L. E. Scott-Denton, K. Sparks, and T. E. Huxman (2002), Carbon sequestration in a high-elevation, subalpine forest, *Global Change Biol.*, *8*, 459–478.

Monson, R. K., J. P. Sparks, T. N. Rosenstiel, L. E. Scott-Denton, T. E. Huxman, P. C. Harley, A. A. Turnipseed, S. P. Burns, B. Backlund, and J. Hu (2005), Climatic influences on net ecosystem CO_2 exchange during the transition from wintertime carbon source to springtime carbon sink in a high-elevation, subalpine forest, *Oecologia*, *146*, 130–147.

Monson, R. K., M. R. Prater, J. Hu, S. P. Burns, J. P. Sparks, K. L. Sparks, and L. E. Scott-Denton (2010), Tree species effects on ecosystem water-use efficiency in a high-elevation, subalpine forest, *Oecologia*, *162*(2), 491–504.

Moore, D. J. P., J. Hu, W. J. Sacks, D. S. Schimel, and R. K. Monson (2008), Estimating transpiration and the sensitivity of carbon uptake to water availability in a subalpine forest using a simple ecosystem process model informed by measured net CO_2 and H_2O fluxes, *Agric. For. Meteorol.*, *148*, 1467–1477.

Naegler, T., and I. Levin (2009), Biosphere-atmosphere gross carbon exchange flux and the $\delta^{13}CO_2$ and $\Delta^{14}CO_2$ disequilibria constrained by the biospheric excess radiocarbon inventory, *J. Geophys. Res.*, *114*, D17303, doi:10.1029/2008JD011116.

Neill, C., B. Fry, J. M. Melillo, P. A. Steudler, J. F. L. Moraes, and C. C. Cerri (1996), Forest- and pasture-derived carbon contributions to carbon stocks and microbial respiration of tropical pasture soils, *Oecologia*, *107*(1), 113–119.

Ogee, J., P. Peylin, P. Ciais, T. Bariac, Y. Brunet, P. Berbigier, C. Roche, P. Richard, G. Bardoux, and J.-M. Bonnefond (2003), Partitioning net ecosystem carbon exchange into net assimilation and respiration using $^{13}CO_2$ measurements: A cost-effective sampling strategy, *Global Biogeochem. Cycles*, *17*(2), 1070, doi:10.1029/2002GB001995.

Pan, Y., et al. (2011), A large and persistent carbon sink in the world's forests, *Science*, *333*(6045), 988–993.

Pataki, D. E., R. Oren, and W. K. Smith (2000), Sap flux of co-occurring species in a western subalpine forest during seasonal soil drought, *Ecology*, *81*(9), 2557–2566.

Pataki, D. E., J. R. Ehleringer, L. B. Flanagan, D. Yakir, D. R. Bowling, C. J. Still, N. Buchmann, J. O. Kaplan, and J. A. Berry (2003), The application and interpretation of Keeling plots in terrestrial carbon cycle research, *Global Biogeochem. Cycles*, *17*(1), 1022, doi:10.1029/2001GB001850.

Ponton, S., L. B. Flanagan, K. P. Alstad, B. G. Johnson, K. Morgenstern, N. Kljun, T. A. Black, and A. G. Barr (2006), Comparison of ecosystem water-use efficiency among Douglas-fir forest, aspen forest and grassland using eddy covariance and carbon isotope techniques, *Global Change Biol.*, *12*(2), 294–310.

Raczka, B. M., et al. (2013), Evaluation of continental carbon cycle simulations with North American flux tower observations, *Ecol. Monogr.*, *83*(4), 531–556.

Randerson, J. T., G. J. Collatz, J. E. Fessenden, A. D. Munoz, C. J. Still, J. A. Berry, I. Y. Fung, N. Suits, and A. S. Denning (2002), A possible global covariance between terrestrial gross primary production and ^{13}C discrimination: Consequences for the atmospheric ^{13}C budget and its response to ENSO, *Global Biogeochem. Cycles*, *16*(4), 1136, doi:10.1029/2001GB001845.

Reichstein, M., et al. (2005), On the separation of net ecosystem exchange into assimilation and ecosystem respiration: Review and improved algorithm, *Global Change Biol.*, *11*(9), 1424–1439.

Revelle, R., and H. E. Suess (1957), Carbon dioxide exchange between atmosphere and ocean and the question of an increase of atmospheric CO_2 during the past decades, *Tellus*, *9*, 18–27.

Rhoades, C. C., et al. (2013), Biogeochemistry of beetle-killed forests: Explaining a weak nitrate response, *Proc. Natl. Acad. Sci. U.S.A.*, *110*, 1756–1760.

Richardson, A. D., D. Y. Hollinger, D. B. Dail, J. T. Lee, J. W. Munger, and J. O'Keefe (2009), Influence of spring phenology on seasonal and annual carbon balance in two contrasting New England forests, *Tree Physiol.*, *29*(3), 321–331.

Riveros-Iregui, D. A., J. Hu, S. P. Burns, D. R. Bowling, and R. K. Monson (2011), An interannual assessment of the relationship between the stable carbon isotopic composition of ecosystem respiration and climate in a high-elevation subalpine forest, *J. Geophys. Res.*, *116*, G02005, doi:10.1029/2010JG001556.

Roden, J. S., and J. R. Ehleringer (2007), Summer precipitation influences the stable oxygen and carbon isotopic composition of tree-ring cellulose in *Pinus ponderosa*, *Tree Physiol.*, *27*(4), 491–501.

Sabine, C. L., et al. (2004), The oceanic sink for anthropogenic CO_2, *Science*, *305*(5682), 367–371.

Schaeffer, S. M., J. B. Miller, B. H. Vaughn, J. W. C. White, and D. R. Bowling (2008a), Long-term field performance of a tunable diode laser absorption spectrometer for analysis of carbon isotopes of CO_2 in forest air, *Atmos. Chem. Phys.*, *8*, 5263–5277.

Schaeffer, S. M., D. E. Anderson, S. P. Burns, R. K. Monson, J. Sun, and D. R. Bowling (2008b), Canopy structure and atmospheric flows in relation to the δ^{13}C of respired CO_2 in a subalpine coniferous forest, *Agric. For. Meteorol.*, *148*, 592–605.

Schimel, D. S., B. H. Braswell, E. A. Holland, R. McKeown, D. S. Ojima, T. H. Painter, W. J. Parton, and A. R. Townsend (1994), Climatic, edaphic, and biotic controls over storage and turnover of carbon in soils, *Global Biogeochem. Cycles*, *8*(3), 279–293.

Schnyder, H., and F. A. Lattanzi (2005), Partitioning respiration of C_3-C_4 mixed communities using the natural abundance ^{13}C approach—Testing assumptions in a controlled environment, *Plant Biol.*, *7*(6), 592–600.

Scholze, M., J. O. Kaplan, W. Knorr, and M. Heimann (2003), Climate and interannual variability of the atmosphere-biosphere [13]CO_2 flux, *Geophys. Res. Lett.*, *30*(2), 1097, doi:10.1029/2002GL015631.

Schuur, E. A. G., et al. (2008), Vulnerability of permafrost carbon to climate change: Implications for the global carbon cycle, *BioScience*, *58*, 701–714.

Schwalm, C. R., et al. (2010), Assimilation exceeds respiration sensitivity to drought: A FLUXNET synthesis, *Global Change Biol.*, *16*(2), 657–670.

Scott-Denton, L. E., K. L. Sparks, and R. K. Monson (2003), Spatial and temporal controls of soil respiration rate in a high-elevation, subalpine forest, *Soil Biol. Biochem.*, *35*, 525–534.

Shim, J. H., H. H. Powers, C. W. Meyer, W. T. Pockman, and N. McDowell (2011), The role of interannual, seasonal, and synoptic climate on the carbon isotope ratio of ecosystem respiration at a semiarid woodland, *Global Change Biol.*, *17*(8), 2584–2600.

Stephens, B. B., N. L. Miles, S. J. Richardson, A. S. Watt, and K. J. Davis (2011), Atmospheric CO_2 monitoring with single-cell NDIR-based analyzers, *Atmos. Meas. Tech.*, *4*(12), 2737–2748.

Still, C. J., J. A. Berry, G. J. Collatz, and R. S. DeFries (2003), Global distribution of C_3 and C_4 vegetation: Carbon cycle implications, *Global Biogeochem. Cycles*, *17*(1), 1006, doi:10.1029/2001GB001807.

Stoy, P. C., et al. (2009), Biosphere-atmosphere exchange of CO_2 in relation to climate: A cross-biome analysis across multiple time scales, *Biogeosciences*, *6*(10), 2297–2312.

Suess, H. E. (1955), Radiocarbon concentration in modern wood, *Science*, *122*(3166), 415–417.

Takahashi, T., et al. (2009), Climatological mean and decadal change in surface ocean pCO_2, and net sea–air CO_2 flux over the global oceans, *Deep Sea Res., Part II*, *56*(8–10), 554–577.

Tans, P. P., J. A. Berry, and R. F. Keeling (1993), Oceanic ^{13}C/^{12}C observations: A new window on ocean CO_2 uptake, *Global Biogeochem. Cycles*, *7*(2), 353–368.

Tcherkez, G., R. Bligny, E. Gout, A. Mahé, M. Hodges, and G. Cornic (2008), Respiratory metabolism of illuminated leaves depends on CO_2 and O_2 conditions, *Proc. Natl. Acad. Sci. U.S.A.*, *105*(2), 797–802.

Tcherkez, G., A. Mahé, and M. Hodges (2011), ^{12}C/^{13}C fractionations in plant primary metabolism, *Trends Plant Sci.*, *16*(9), 499–506.

Torn, M. S., S. C. Biraud, C. J. Still, W. J. Riley, and J. A. Berry (2011), Seasonal and interannual variability in ^{13}C composition of ecosystem carbon fluxes in the U.S. Southern Great Plains, *Tellus, Ser. B*, *63*(2), 181–195.

Trumbore, S. (2009), Radiocarbon and soil carbon dynamics, *Annu. Rev. Earth Planet. Sci.*, *37*, 47–66.

van der Velde, I. R., J. B. Miller, K. Schaefer, K. A. Masarie, S. Denning, J. W. C. White, P. P. Tans, M. C. Krol, and W. Peters (2013), Biosphere model simulations of interannual variability in terrestrial ^{13}C/^{12}C exchange, *Global Biogeochem. Cycles*, *27*, 637–649, doi:10.1002/gbc.20048.

Vaughn, B. H., J. Miller, D. F. Ferretti, and J. W. C. White (2004), Stable isotope measurements of atmospheric CO_2 and CH_4, in *Handbook of Stable Isotope Analytical Techniques*, edited by P. A. de Groot, pp. 272–304, Elsevier, Amsterdam.

Warren, C. R., J. F. McGrath, and M. A. Adams (2001), Water availability and carbon isotope discrimination in conifers, *Oecologia*, *127*(4), 476–486.

Welp, L. R., R. F. Keeling, H. A. J. Meijer, A. F. Bollenbacher, S. C. Piper, K. Yoshimura, R. J. Francey, C. E. Allison, and M. Wahlen (2011), Interannual variability in the oxygen isotopes of atmospheric CO_2 driven by El Niño, *Nature*, *477*(7366), 579–582.

Werner, C., and A. Gessler (2011), Diel variations in the carbon isotope composition of respired CO_2 and associated carbon sources: A review of dynamics and mechanisms, *Biogeosciences*, *8*(9), 2437–2459.

Wilson, K. B., D. D. Baldocchi, and P. J. Hanson (2001), Leaf age affects the seasonal pattern of photosynthetic capacity and net ecosystem exchange of carbon in a deciduous forest, *Plant Cell Environ.*, *24*(6), 571–583.

Wingate, L., J. Ogee, R. Burlett, A. Bosc, M. Devaux, J. Grace, D. Loustau, and A. Gessler (2010), Photosynthetic carbon isotope discrimination and its relationship to the carbon isotope signals of stem, soil and ecosystem respiration, *New Phytol.*, *188*(2), 576–589.

Yakir, D. (2004), The stable isotopic composition of atmospheric CO_2, in *Treatise on Geochemistry*, The Atmosphere, vol. 4, edited by R. F. Keeling, pp. 175–212, Elsevier, Amsterdam.

Yakir, D. (2011), The paper trail of the ^{13}C of atmospheric CO_2 since the industrial revolution period, *Environ. Res. Lett.*, *6*, 034,007, doi:10.1088/1748-9326/1086/1083/034007.

Yakir, D., and X. F. Wang (1996), Fluxes of CO_2 and water between terrestrial vegetation and the atmosphere estimated from isotope measurements, *Nature*, *380*, 515–517.

Zarter, C. R., B. Demmig-Adams, V. Ebbert, I. Adamska, and W. W. Adams III (2006a), Photosynthetic capacity and light harvesting efficiency during the winter-to-spring transition in subalpine conifers, *New Phytol.*, *172*(2), 283–292.

Zarter, C. R., W. W. Adams III, V. Ebbert, D. J. Cuthbertson, I. Adamska, and B. Demmig-Adams (2006b), Winter down-regulation of intrinsic photosynthetic capacity coupled with up-regulation of Elip-like proteins and persistent energy dissipation in a subalpine forest, *New Phytol.*, *172*(2), 272–282.

Zhang, J., T. J. Griffis, and J. M. Baker (2006), Using continuous stable isotope measurements to partition net ecosystem CO_2 exchange, *Plant Cell Environ.*, *29*(4), 483–496.

Zhu, B., and W. Cheng (2011), ^{13}C isotope fractionation during rhizosphere respiration of C_3 and C_4 plants, *Plant Soil*, *342*, 277–287.

Zobitz, J. M., J. P. Keener, H. Schnyder, and D. R. Bowling (2006), Sensitivity analysis and quantification of uncertainty for isotopic mixing relationships in carbon cycle research, *Agric. For. Meteorol.*, *136*(1–2), 56–75.

Zobitz, J. M., S. P. Burns, M. Reichstein, and D. R. Bowling (2008), Partitioning net ecosystem carbon exchange and the carbon isotopic disequilibrium in a subalpine forest, *Global Change Biol.*, *14*(8), 1785–1800.